كلية الهندسة بشبرا
FACULTY OF ENGINEERING AT SHOUBRA
ERJ
PRINT ISSN 3009-6049
ONLINE ISSN 3009-6022

ENGINEERING RESEARCH JOURNAL (ERJ)
Volume (53) Issue (4)
October. 2024, pp:279-289
https://erjsh.journals.ekb.eg

Investigation of the performance of RC slabs using hybrid reinforcement of geogrid and steel reinforcement

Eslam Essam Saleh[*1] ; Ahmed Abdel-Fatah Mahmoud [1] ; Mohamed Ahmed Salama [1] ; Amr Mohamed Mohamed [2]

[1]Department of Civil Engineering, Faculty of Engineering , Ain Shams University, Cairo, Egypt.
[2] Reinforced Concrete Structures, Faculty of Engineering, Al-Shrouk Academy.
[*] Corresponding Author.
E-mail: islam.essam1966@gmail.com; ahmed.m5882@gmail.com; drmdsalama@icloud.com; a.elsayed@sha.edu.eg.

Abstract: This article explores the impact of uniaxial geogrid type and steel reinforcement bars on the flexural behavior of two-way solid slabs. It uses analytical, numerical, and experimental studies on eight square slab specimens, with uniform loads applied until failure. The study classifies the specimens into five groups based on studied parameters. The investigated parameters were the effect of using the geogrid (with or without geogrid), the number of geogrid layers , the dimensions of the geogrid layer, and its position through the slab thickness. The study measured cracks and failure loads, deflections, failure modes, crack propagation, and patterns, and evaluated the ductility features of all specimens using displacement ductility factors. The experimental results showed that using uniaxial geogrid meshes as a reinforcement for two-way concrete slab was more reliable than using conventional steel bars. This resulted in a 13% increase in failure load, 138% increase in initial stiffness, and 85% increase in energy absorption.Also, using two layers of geogrid above the steel bars, the slab's failure load and energy absorption increased by 8% and 12%, respectively, compared to a slab reinforced with three layers of geogrid above the steel bars. Different analysis methods were employed to verify experimental results based on the nominal flexural strength of the ECP 203-19 code[1]. The results showed that the ECP 203-19 code should be considered as a good method to find the slab's ultimate load, where the average and the standard deviation were 96% and 19%, respectively. The comparison between the load-deflection curves, failure load, and crack patterns from the experimental and numerical specimen (S8) is in good agreement with more than 95%.

Keywords: Analytical study; Experimental investigation; Numerical analysis; Geogrid; RC; Slabs; ANSYS program.

1. INTRODUCTION

One of the most commonly used structural elements in any building is reinforced concrete (RC) slabs. Structural concrete elements' characteristics can be improved by using polymeric materials. Fiber composites made of glass, carbon, and steel are examples of polymeric materials that act as reinforcement. These materials can also be made from geosynthetic materials, such as geogrids and geocells. Geosynthetics are applied to structural elements by using geogrids in concrete structures. In addition to stabilizing and confining soil-retaining structures, geogrids are employed as reinforcement for asphalt concrete layers and to reduce the pavement's progressive cracking. One type of geosynthetic is geogrid; these types are all primarily made of polymeric materials. It can be found that polyester, polyethylene, polypropylene, or polystyrene provide tensile strength. There are three types of geogrids: triaxial, uniaxial, and biaxial. Biaxial geogrids were employed in roadway

applications, whereas in grade separation applications, such as steep slopes, uniaxial geogrids were employed. When constructing a road in a region with loose or sandy soil, triaxial geogrids are used. Applying geogrids in conjunction with concrete as a reinforcing material opened up new possibilities for using geosynthetics in structural engineering. Many investigations examine the impact of geogrid, either with or without steel reinforcement, on structural elements constructed from reinforced concrete [2-4]. So, a few studies have been done on the behavior of structural elements that have been strengthened or reinforced by geogrids. This study aims to investigate the reinforcing properties of geogrid in two-way solid slabs made from reinforced concrete, either with or without steel bars.

The subsequent articles describe how different types of geogrids can be used as reinforcement materials in many structural elements. M. Abd-El Mohsen [5] studied self-compacted concrete prisms reinforced with geogrids and their flexural behavior. Concrete prisms were reinforced using three different types of geogrids (uniaxial, biaxial, and triaxial). One, two, and three layers were used for each type of geogrid. M. Abd-El Mohsen [5] concluded that each type of geogrid reinforcement delivers large deformation values, increased absorbed energy, and ductile behavior in the post-cracking phase. Also, uniaxial geogrid exhibits better flexural behavior than biaxial geogrid. Fares et al. [6] examined the potential for reinforcing high-strength self-compacted concrete slabs with geogrids to improve their tensile strength and ductility. Also, two kinds of geogrid surface modification methods are offered to strengthen the connection between the geogrid layers and the cement matrix. Fares et al. [6] concluded that, by comparing the treated and untreated specimens, the chemical treatment increased the examined slab's ultimate flexural loading capacity by approximately 9% for one geogrid layer and 13% for two geogrid layers. The ultimate flexural loading capacity was reduced, while the slab's ductility was significantly improved by adding more geogrid layers. Rajeshkumar et al. [7] studied how steel and biaxial geogrid-reinforced concrete slabs behave in comparison, and the fundamental characteristics of concrete components and geosynthetics were examined. Rajeshkumar et al. [7] indicated that the geogrid behaved well and gave good results when used in RC slabs. In comparison to the steel-reinforced slab, the geogrid-reinforced slab's load-carrying capacity, deflection, and energy absorption increased by 25%, 7%, and 23%, respectively.

Haggag and Abd Elsalam [8] examined the flexural behavior of two-way solid slabs with GFRP bars as reinforcement, both numerically and experimentally. Nine slabs with thicknesses of 60 and 70 mm were used and divided into two groups, A and B. Haggag and Abd Elsalam [8] concluded that for slabs with the same reinforcing ratio (0.53%), the ultimate capacity of the slab increased by 10% when the slab thickness increased from 60 mm to 70 mm. Regarding the load-deflection relationship, the load-strain relationship, and the crack patterns for the experimental specimens, the numerical models created with ANSYS software produced almost identical results. Itani et al. [9] studied thin concrete overlays' performance. Itani et al. [9] look into the use of geogrids as a reinforcement-crack arresting layer. Itani et al. [9] study has been done to increase strength and ductility and control crack patterns. Itani et al. [9] concluded that, for specimens under direct tension, many failure modes were noted. While the geogrid reinforcement significantly increased the post-cracking durability. The plain specimens showed brittle failure. In contrast, the reinforced specimens displayed larger deformations and an increase in strength, followed by cracks.Also,there are many different researches studied the effect of hyprid concrete slabs with different geogrid types as reinforced or strenghing material . Like, R. Al-Rousan [10], X.Wang et al. [11], O. Aljidda et al. [12], U. Bishnoi et al. [13], Y. Zheng et al. [14], and F. Hassan et al. [15],all of them concluded that the effect of geogrid as reinforced or strenghing material increases the ductility and strength for slabs.

From the previous literature review, there is little research on the effect of geogrid as a hybrid reinforcement in RC slabs. So, this study will focus on and introduce more information about the flexural behavior of two-way solid slabs by using uniaxial geogrid as a hybrid reinforcement with or without steel bars.

2. Experimental Investigation

2.1 Tested Specimens Description

The experimental program consisted of eight concrete slabs. The specimens were divided into five groups, including the control slab specimens. Each group consisted of several slab specimens to study different parameters, as shown in Table 1. Two control slabs were used for the comparison, where one concrete slab was reinforced with steel bars only and another was reinforced with geogrid only. In addition, the experimental program involves evaluating six slab specimens reinforced with geogrid and steel bars. The slabs are squares with a total length of 1750 mm and a center-to-center span of 1450 mm. The specimens have identical thicknesses of 100 mm. The slabs rested on four marginal steel I-beams with dimensions equal to 150 mm flange width and 300 mm web height, as illustrated in Figure 1. Four square steel plates of 200 mm in length and 20 mm in thickness distribute the applied load uniformly over the slab top surface, as illustrated in Figure 1. As shown in Figure 1, three LVDTs are positioned at 25%, 50%, and 75% of the loaded slabs' span.

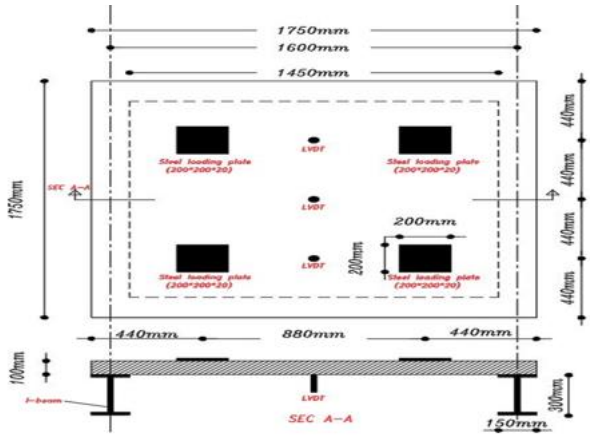

Fig 1: Specimen dimensions, loading and bearing steel plates, and LVDT locations.

2.2 Mixture composition and material properties

The combination of materials used to cast the tested slabs was designed according to the Egyptian codes ECP 203-2019 [1] and ASTM [16-21]. Table 2 shows the proportions of components by weight per 1 m^3 of concrete to achieve the charachteristic compressive strength (f_{cu}) 30 MPa, according to ASTM [16] . To determine the concrete's cubic compressive strength (f_{cu}), standard cubes were extracted from the mix for every specimen . The splitting tensile strength (f_{ct}) was also estimated using cylinders with dimensions of 150 x 300 mm, according to ASTM [18]. The mechanical properties of concrete for each tested specimen in tension and compression are shown in Table 3. The stress-strain curve for uniaxial geogrid is displayed in Figure 3, according to ASTM [19]. The yield and ultimate strength according to ASTM [20-21] for the steel bars of diameter 8 mm used in this study are 337 MPa and 458 MPa, respectively.

2.3 Test setup, instrumentation, and procedures

The specimens were tested in a stiff steel frame in the reinforced concrete laboratory at the Higher Institute of Engineering-Al Shorouk. The slabs rested on four steel I-beams. A 600 kN hydraulic jack was used. The test setup was designed to distribute the loads uniformly over the four steel loading plates. Figure 1 shows the linear variable differential transducers (LVDT) measure the deflection at 25%, 50%, and 75% of the total span of the slab. A 2-D,and 3-D view for test setup is shown in Figure 2 . Furthermore, at each loading step, the cracks were marked.The loads and the corresponding deflections were recorded by the data acquisition system connected to the load cell, a computer, and a monitor. All tested instruments are calibrated and reset to zero before the test.

Fig 2: A 2-D,and 3-D view for test setup.

Table 1: Details of the tested specimens.

Group no.	Slab symbol	Reinforcement type	Number and diameter of steel bars/direction	Number of geogrid layers in each direction	geogrid dimensions	geogrid position in the slab section	Remarks
A	Slab 1	Only steel bars	10Ø8	-	-	-	Study the effect of reinforcement type.
	Slab 2	Only geogrid	-	1	Full slab dimension	20mm from the bottom of the slab	
B	Slab 1	Only steel bars	10Ø8	-	-	-	Study the effect of using geogrid.
	Slab 2	Only geogrid	-	1	Full slab dimension	20 mm from the bottom of the slab	
	Slab 3	Steel and geogrid	10Ø8	1	Full slab dimension	At the top of the steel bars	
C	Slab 3	Steel and geogrid	10Ø8	1	Full slab dimension	At the top of the steel bars	Study the effect of the number of geogrid layers.
	Slab 4	Steel and geogrid	10Ø8	2	Full slab dimension	At the top of the steel bars	
	Slab 5	Steel and geogrid	10Ø8	3	Full slab dimension	At the top of the steel bars	
D	Slab 3	Steel and geogrid	10Ø8	1	Full slab dimension	At the top of the steel bars	Study the effect of geogrid dimensions.
	Slab 6	Steel and geogrid	10Ø8	1	Strips 100 mm wide at 200 mm spacing	At the top of the steel bars	
	Slab 7	Steel and geogrid	10Ø8	1	Strips 100 mm wide at 100 mm spacing	At the top of the steel bars	
E	Slab 3	Steel and geogrid	10Ø8	1	Full slab dimension	At the top of the steel bars	Study the effect of geogrid position.
	Slab 8	Steel and geogrid	10Ø8	1	Full slab dimension	At the bottom of the steel bars	

Table 2: The proportions of the concrete mix per m^3.

Specimen	Water (liter)	Cement (kg)	Fine aggregate (kg)	Coarse aggregate (kg)	
				10 mm	20 mm
For all slabs /m^3	150	350	682.25	1275.8	-
Properties	Normal potable water was devoid of Pollutants, or chemicals.	Ordinary Portland cement (OPC) (CEM I42.5)	Clean and clear from biological materials	- Crushed limestone. - The surface texture was uniform and smooth.	

Table 3: Mechanical properties of concrete in tension and compression.

Specimen symbol	(f_{ct}) (MPa)	($f`_c$) (MPa)	(f_{cu}) (MPa)
Slab 1	2.9	25	30
Slab 2	3.2	24	30
Slab 3	3.2	23	29
Slab 4	3.2	24	31
Slab 5	2.9	23	29
Slab 6	3.0	24	30
Slab 7	3.1	23	30
Slab 8	3.0	25	31
Average	3.0	24	30

Where:

f_t: is the concrete's splitting tensile strength.

$f`_c$; is the concrete's cylindrical compressive strength.

f_{cu}: is the concrete's cubic compressive strength.

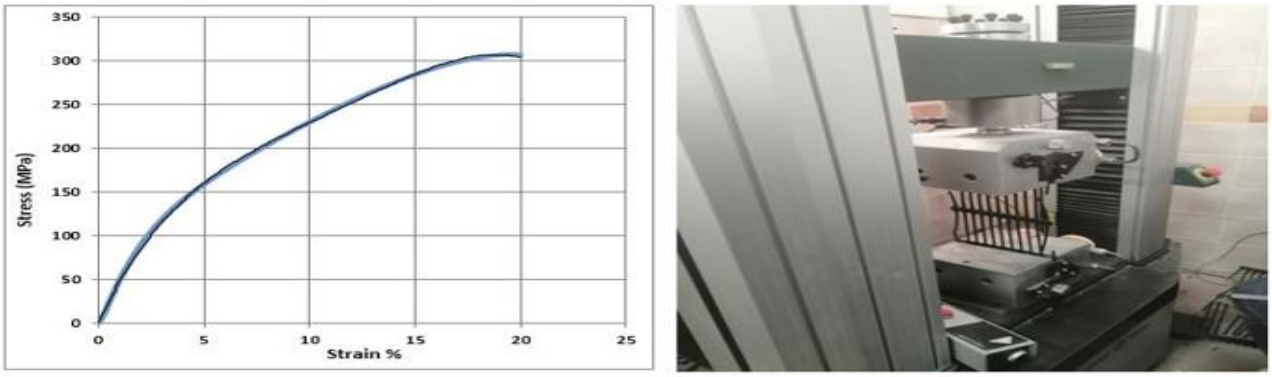

(a) Geogrid stress-strain curve. (b) Test of geogrid.

Fig 3: Geogrid stress-strain curve and its tension test.

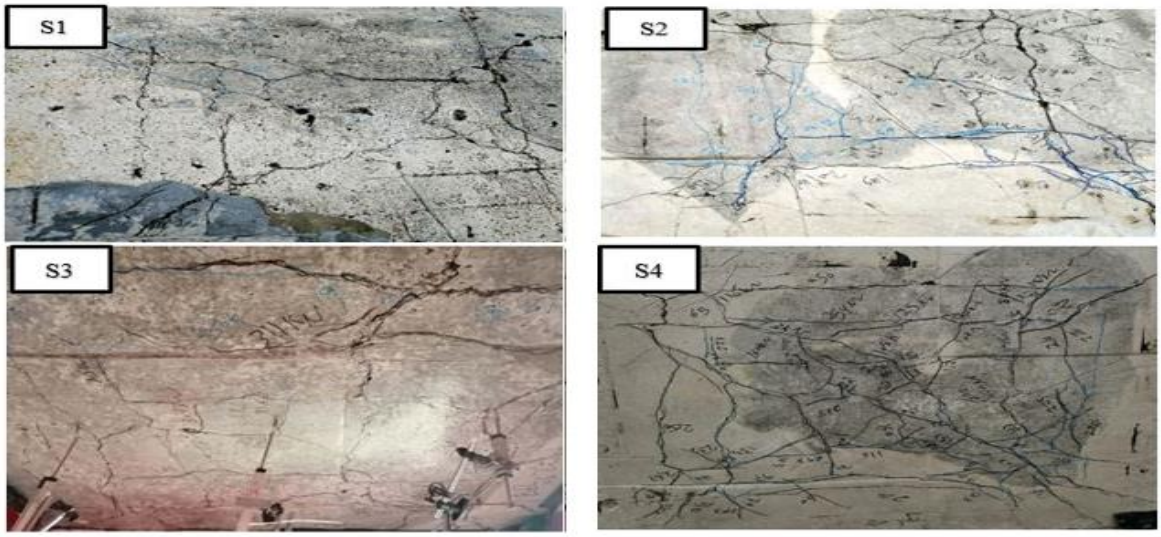

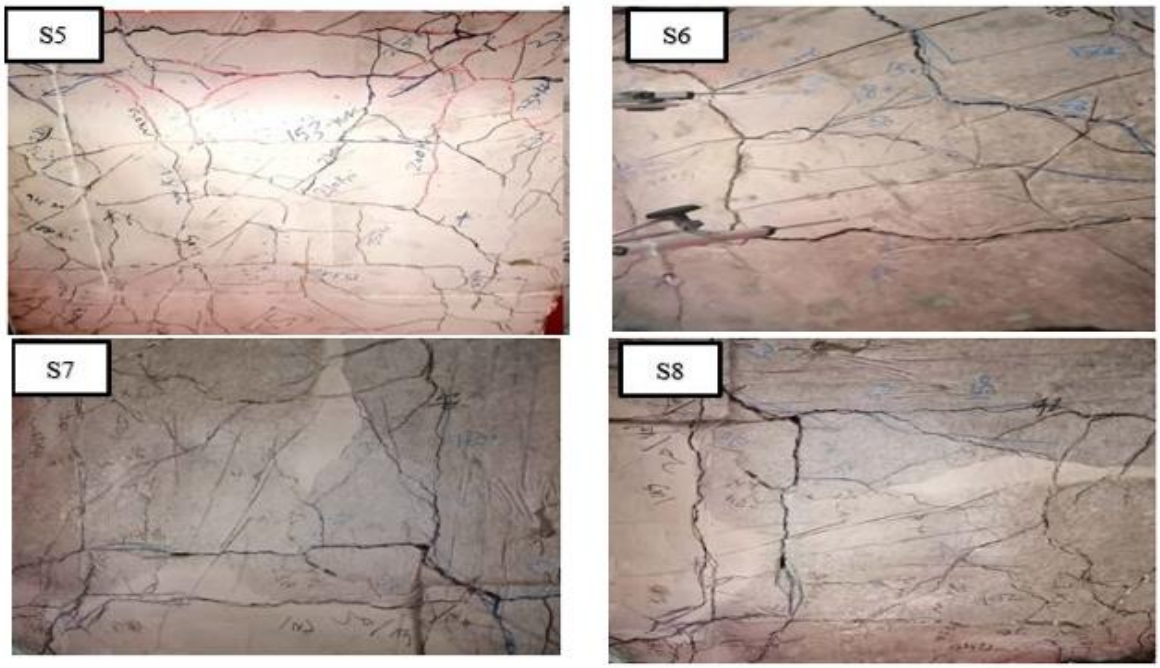

Fig 4: Crack patterns for all specimens

Table 4: The first crack and failure loads for all tested slabs.

Slab symbol	P_{cr} (kN)	P_f (kN)
Slab 1	77	220
Slab 2	44	248.9
Slab 3	55	316
Slab 4	46	279
Slab 5	50	258
Slab 6	90	334
Slab 7	123	290
Slab 8	120	252

Where: P_{cr}: is the experiment's first crack load.
P_f: is the experiment's failure load.

3.Analysis of the Experimental Results

3.1Crack patterns, first crack, and failure loads

All specimens failed due to flexural failure. The mode of failure and crack patterns for all specimens are displayed in Figure 4. The first crack and failure loads for all tested slabs are shown in Table 4.

3.2 Load-deflection curves and deflected shapes

Figure 5 shows the load-deflection curves at mid-span for all tested slabs. Figure 6 illustrates the deflected shapes for all slabs at (0, 0.25 L, 0.5 L, 0.75 L, and L), where L is the center-to-center span length at a constant load of 220 kN, representing the smallest failure load of all tested specimens as shown in Table 4.

3.3 Secant stiffness (S.S.), displacement ductility (D.D.), and toughness (T)

Table 5 shows values of secant stiffness (S.S.), which equals the ratio between ultimate load to ultimate deflection as shown in Figures 7-a, and toughness (T), which equals the area under load-deflection curves for tested slabs up to failure as shown in Figures 7-b . Displacement ductility (D.D.) is the ratio between the deflection at 90% of the ultimate load in the

descending branch and that in the ascending branch as shown in Figure 7-c. Table 5 shows that toughness, secant stiffness, and displacement ductility increased by about 71%, 113%, and 44%, respectively, due to the use of the geogrid layers, depending on the properties of the used geogrid layers (thickness, number, dimensions, and position).

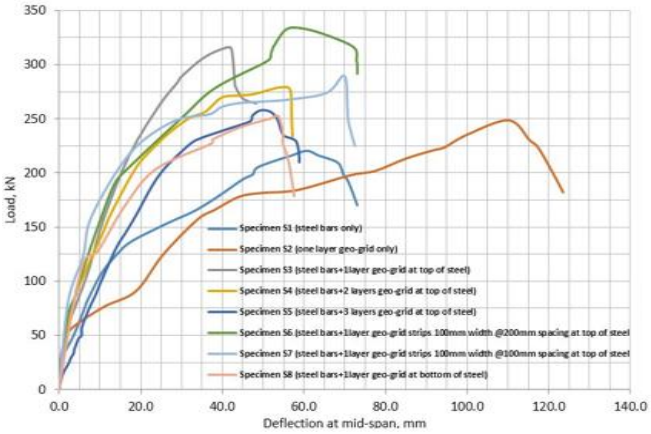

Fig 5: Load-mid-span deflection curves for all slabs.

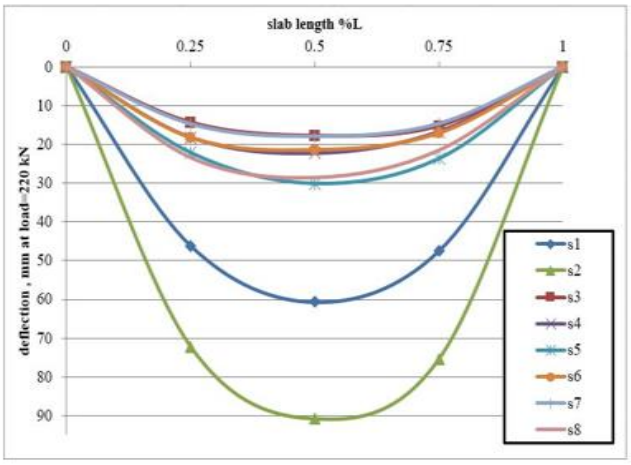

Fig 6: The deflected shapes for all slabs.

Table 5: Secant stiffness, displacement ductility, and toughness.

Slab symbol	(S.S.)	(D.D.)	(T)
	(kN/mm)	(mm/mm)	(kN.mm)
Slab 1	3.63	1.47	17698
Slab 2	2.26	1.24	32753
Slab 3	7.75	1.48	17241
Slab 4	5.16	1.77	18864
Slab 5	5.24	1.64	16924
Slab 6	5.64	1.47	28989
Slab 7	4.15	1.78	24863
Slab 8	4.69	1.46	16107

(a) where: S.S.: is the secant stiffness. , D.D.: is the displacement ductility. , and T: is the toughness.

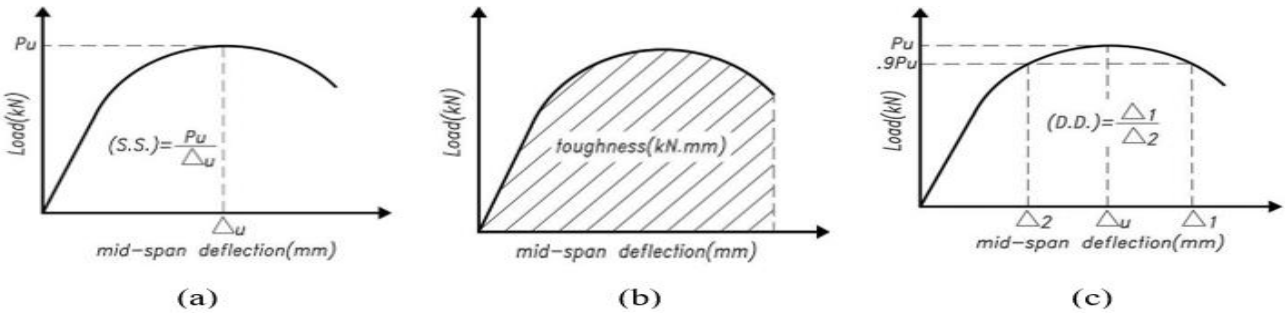

Fig 7: Charts illustrated the definition of the following , (a) Secant stiffness (S.S.) relationship , (b) Toughness (T) relationship , and (c) Displacement ductility (D.D.) relationship.

Table 6: Comparison between predicted ultimate loads from different analytical methods and experimental failure loads.

Slab symbol	P exp	$P_{Grash.}$	PGrash / Pexp	P Marc.	PMarc / Pexp	P ECP	P ECP / Pexp	P SAP	P SAP / Pexp	P Yield	P Yield / Pexp
	(kN)	(kN)	%	(kN)	%	(kN)	%	(kN)	%	(kN)	%
Slab 1	220.11	147.35	66.94	251.30	114.17	210.03	95.42	153.20	69.60	220.56	100.20
Slab 2	248.82	110.8	44.53	188.90	75.92	157.92	63.47	115.17	46.29	165.84	66.65
Slab 3	315.81	194.01	61.43	330.85	104.76	276.54	87.57	201.70	63.87	290.40	91.95
Slab 4	279.2	219.19	78.51	373.80	133.88	312.42	111.90	227.83	81.60	328.08	117.51
Slab 5	258	235.22	91.17	401.13	155.48	335.27	129.95	244.50	94.77	352.08	136.47
Slab 6	333.82	165	49.43	281.37	84.29	235.17	70.45	171.50	51.37	246.96	73.98
Slab 7	289.71	174.8	60.34	298.05	102.88	249.10	85.98	181.67	62.71	261.60	90.30
Slab 8	252.3	210.05	83.25	358.20	141.97	299.40	118.67	218.33	86.54	314.40	124.61
Average%			66.95		114.17		95.43		69.59		100.21
Standard Dev. S.D.%			16.34		22.21		18.56		13.53		24.47

4. Analytical Study

Table 6 shows the comparison of the ultimate failure load from different analytical methods and the experimental failure load P_{exp}. The analytical methods used are Marcou's, Grashoff's, and yield line theories, ECP 203-19 [1], and Sap 2000. From Table 6, yield line theory could be considered the best analytical method to simulate two-way solid slabs with or without geogrid or steel reinforcement bars, where the average is 100.2%. The results also showed that the ECP 203-19 [1] code should be considered a good method to find the slab ultimate load, where the average and the standard deviation were 96% and 19%, respectively.Also, ECP 203-19 code equations [1] for RC slabs containing steel bars only are shown below from EQ (1) to EQ (9). Also, Figure 8 shows the stress and strain distribution along arectangular reinforced concrete section.

4.1 ECP 203-19 code equations

[1] for RC slabs containing steel bars only

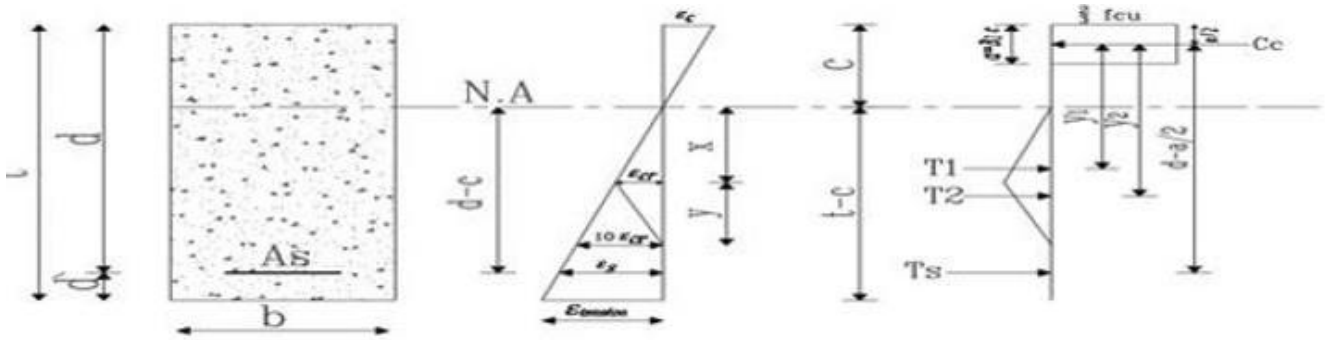

Fig 8:The stress and strain distribution along arectangular reinforced concrete section.

$$Mu\ internal = \left[Ts\left(d - \frac{a}{2}\right) + T1\ y1 + T2\ y2 \right] 10^{-6} \quad \text{EQ (1)}$$

$$M_{u\ internal} = M_{u\ external}$$

For two-way solid slabs, the maximum mid-span moment, according to Grashoff ' s theory,

$$Mu\ external\ (Grashoff) = \frac{\beta\, w\, l^2}{8} \quad , \beta = .5 \quad \text{EQ (2)}$$

$$PGrash = w\, l^2 \quad \text{EQ (3)}$$

According to Marcou's theory,

$$Mu\ external\ (Marcous) = \frac{\beta\, w\, l^2}{8} \quad , \beta = .292 \quad \text{EQ (4)}$$

$$PMarc = w\, l^2 \quad \text{EQ(5)}$$

Where:

W: uniformly distributed load on slab (kN/mm²),

L: the total length of span for slab (mm)

Then, according to ECP 208-19 [1],

$$Mu\ external\ (ECP) = \frac{\beta\, w\, l^2}{8} \quad , \beta = .35 \quad \text{EQ (6)}$$

$$PECP = w\, l^2 \quad \text{EQ (7)}$$

Then, according to SAP 2000 output:

$$P\ SAP = \left(\frac{Mu\ external}{\beta}\right) * 10 \quad , \beta = .6 \quad \text{EQ (8)}$$

According to the yield line theory, and for this study case:

$$P\ (Yield\ line) = 24\ Mu\ external \quad \text{EQ (9)}$$

Where: P: is the analytical ultimate load(kN).

5. Numerical Study

The ANSYS V15.0 nonlinear finite element program was implemented to confirm the tested slabs results. The concrete material is idealized with the SOLID 65 element. The loading and bearing steel plates were idealized using SOLID 185 elements. The steel bars and uniaxial geogrid are idealized with LINK180 elements. The supporting system along the slab's bottom edge was idealized by hinged supports, including the constraints at the four corners that restricted movement in the x, y, and z directions, as shown in Figures 9-a and 9-b. The properties of the used materials were mentioned in the previous section concerning the experimental program and shown in Figures 9-c, 9-d, and 3-a.

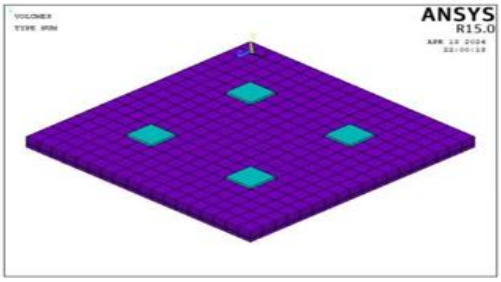

(a) 3-D view of the slab model

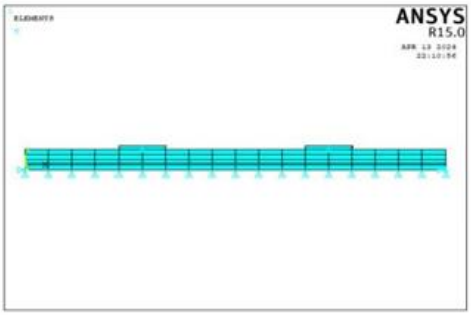

(b) A 2-D view of the slab model.

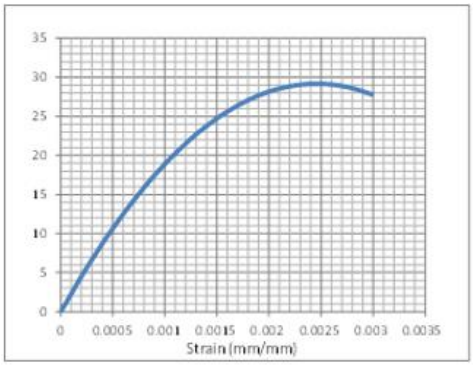

(c) Concrete compressive stress-strain curve.

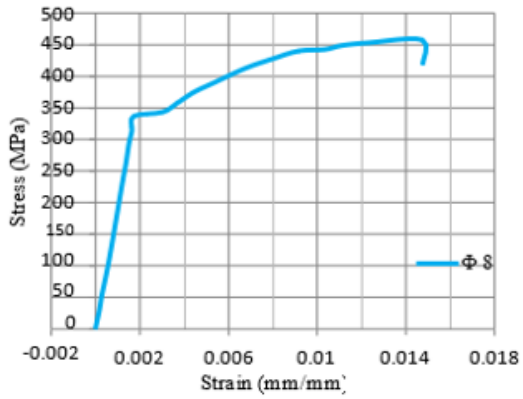

(d) Steel reinforcement bar's stress-strain curve.

Fig 9: Finite element modeling and material idealizations.

5.1. Analysis and Comparison of Results

The comparison of the load-deflection curves for specimen S8 from experimental and numerical data is shown in Figure 10. The numerical ultimate load for slab S8 was 235 kN, compared to the experimental failure load of 252 kN, a conservative percentage equal to 93%. The numerical crack pattern and contour-deformed shape of slab S8 are shown in Figure 11.

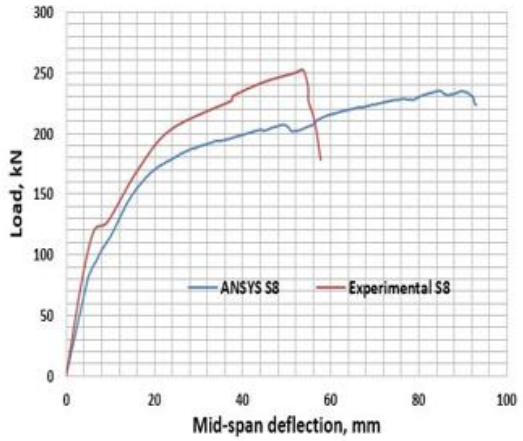

Fig 10: Load-deflection curves for specimen S8: numerical and experimental.

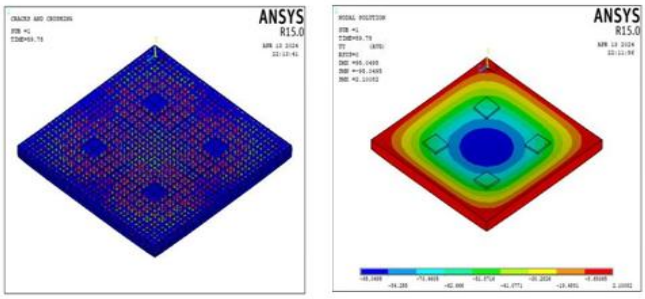

Fig 11: Numerical crack pattern and contour-deformed shape for specimen S8.

6. Conclusions

1- This study shows that the use of uniaxial geogrid type UG-160 as a hybrid reinforcement is an acceptable alternative for steel reinforcement, partially or totally, for offering high performance in tension in two-way solid slabs, where the slab's failure load increased by 13% compared to a specimen reinforced only by the same area of steel bars. Also, the initial stiffness of the slab increased by 138%, while its toughness (energy absorption) increased by 85%.

2- The energy absorption and ultimate load capacity are increased by 7% and 25%, respectively, when using one layer of uniaxial geogrid type UG-160 above the steel reinforcement bars.

3- The use of two layers of geogrid above the steel reinforcement bars increases displacement ductility. When using three layers above the steel bars, the displacement ductility decreased due to the increased ratio of geogrid as reinforcement.

4- Toughness, secant stiffness, and displacement ductility increased by about 71%, 113%, and 44%, respectively, due to the use of the geogrid layers, depending on the properties of the used geogrid layers (thickness, number, dimensions, and position).

5- The results showed that the ECP 203-19 code should be considered a good method to find the slab's ultimate load, where the average and the standard deviation were 95.415% and 18.554%, respectively.

6- The comparison of the load-deflection curves, failure load, and crack patterns from the experimental and numerical ones is in good agreement and almost has identical results, where the numerical model's crack patterns and modes of failure match those of the experimental ones.

References

[1] Egyptian Code of Practice for Design and Construction of Reinforced Concrete Structures. ECP-203, Housing and Building Research Center, Ministry of Building and Construction, Giza Egypt, Chapter4, pp. 25–32. 2019 https://www.cuipcairo.org/en/directory/housing-building-national-research-center

[2] T. J. Vijay, K. R. Kumar, R. Vandhiyan, K. Mahender, and K. Tharani, Performance of geogrid-reinforced concrete slabs under drop weight impact loading, Material Science Engineering, vol. 981, 2022, doi: 10-1088/1757-899X/981/3/032070.

[3] A. S. A. Gabr, Strengthening of reinforced concrete slabs using different types of geogrids, International Journal of Civil Engineering Technology, vol. 10, no. 1, pp. 1851–1861, 2019.

[4] A. J. Whittle and H. I. Ling, Geosynthetics in Construction: Encyclopedia of Materials, Science, and Technology, pp. 1–13, 2002. Doi: 10.1016/b0-08-043152-6/01801-5.

[5] M. Abd-El Mohsen, Flexural behavior of self-compacting concrete prisms reinforced with geogrids, Journal of Engineering Science, Assiut University, vol. 45, no. 4, pp. 422-435, 2017. DOI:10.21608/jesaun.2017.116281

[6] A. E. R. Fares, H. Hassan, and M. Arab, Flexural behavior of high-strength self-compacted concrete slabs containing treated and untreated geogrid reinforcement, Fibers, vol. 8, no. 4, 2020, doi: 10.3390/fib8040023.

[7] K. Rajeshkumar and P. O. Awoyera, G. Shyamala, V. M. Kumar, N. Gurumoorthy, S. Kayikci, L. M. B. Romero, and A. K. Prakash, Structural performance of biaxial geogrid-reinforced concrete slab, International Journal of Civil Engineering, vol. 20, pp. 349–359, 2022. Doi: https://doi.org/10.1007/s40999-021-00668-y.

[8] H. A. Haggag and M. M. Abd Elsalam, Flexural behavior of two-way solid slabs reinforced with GFRP bars, International Journal of Civil Engineering Technology, vol. 11, no. 1, pp. 288–303, 2020. https://papers.ssrn.com/sol3/papers.cfm?abstract_id=3535401

[9] H. Itani, G. Saad, and G. Chehab, Use of geogrid reinforcement for enhancing the performance of concrete overlays: An experimental and numerical assessment, Construction and Building Materials, vol. 124, no. 1, pp. 826–837, 2016. doi.org/10.1016/j.conbuildmat.2016.08.013.

[10] R. Al-Rousan, "Influence of polypropylene fibers on the flexural behavior of reinforced concrete slabs with different opening shapes and sizes," *Struct. Concr.*, vol. 18, no. 6, pp. 986–999, 2017, doi: 10.1002/suco.201600222. https://doi.org/10.1002/suco.201600222

[11] X. Wang, N. M. Ali, L. Ding, J. Shi, and Z. Wu, "Static behavior of RC deck slabs partially prestressed with hybrid fiber reinforced polymer tendons," *Struct. Concr.*, vol. 19, no. 6, pp. 1895–1907, 2018, doi: 10.1002/suco.201700240. https://doi.org/10.1002/suco.201700240

[12] O. Aljidda, A. El, and W. Alnahhal, "Experimental and numerical investigation of the flexural behavior of one – way RC slabs strengthened with near – surface mounted and externally bonded systems," *Constr. Build. Mater.*, vol. 421, no. December 2023, p. 135709, 2024, doi: 10.1016/j.conbuildmat.2024.135709. https://doi.org/10.1016/j.conbuildmat.2024.135709

[13] U. Bishnoi, A. B. D. Roy, and N. Kwatra, "Out of plane performance of novel concrete sandwich panel using different geosynthetics," *Constr. Build. Mater.*, vol. 300, no. January, p. 124186, 2021, doi: 10.1016/j.conbuildmat.2021.124186.https://doi.org/10.1016/j.conbuildmat.2021.124186

[14] Y. Zheng, L. Zhou, S. E. Taylor, and H. Ma, "Serviceability of one-way high-volume fly ash-self-compacting concrete slabs reinforced with basalt FRP bars," *Constr. Build. Mater.*, vol. 217, pp. 108–127, 2019, doi: 10.1016/j.conbuildmat.2019.05.044.https://doi.org/10.1016/j.conbuildmat.2019.05.044

[15] F. Hassan, F. Hejazi, R. Saifulnaz, and M. Rashid, "Strengthening of reinforced concrete slabs using carbon fiber reinforced polymers rods and concrete jacket with a mechanical anchorage system," *Constr. Build. Mater.*, vol. 440, no. July, p. 137464, 2024,doi:10.1016/j.conbuildmat.2024.137464. https://doi.org/10.1016/j.conbuildmat.2024.137464

[16] ASTM C39/C39M-14 (2015), International standard test method for compressive strength of cylindrical concrete specimens. https://www.studocu.com/row/document/stateengineering-university-of-armenia/concrete-design/astm-c39-c39m-14-concrete-design/32367366

[17] ASTM International, Standard Test Method for Static Modulus of Elasticity and Poisson's Ratio of Concrete in Compression, ASTM C469/C469M-14, West Conshohocken (2015), https://www.astm.org/c0469_c0469m-14.html. DOI: 10.1520/C0469_C0469M-14.

[18] ASTM International, Standard Test Method for Splitting Tensile Strength of Cylinders Concrete Specimens ASTM C496-96 (2015). https://www.astm.org/c0496-96.html.

[19] ASTM, D790-02 (2002). Standard test methods for the flexural properties of unreinforced and reinforced plastics and electrical insulating materials. ASTM International, West Conshohocken, PA, USA.

[20] ASTM International, Standard Test Methods and Definitions for Mechanical Testing of Steel Products, ASTM, (2017). West Conshohocken, PA. A370-17a. https://www.astm.org/a0370-17.html.

[21] ASTM E8/ASTM E8m, 2013, Standard Test Method for Tensile Testing of Metallic Materials.https://www.zwickroell.com/industries/metals/metals-standards/metals-tensile-test-astm-e8/ DOI:10.1520/E0008_E0008M-13A.